Tsunematsu *et al. Earth, Planets and Space* (2016) 68:88
DOI 10.1186/s40623-016-0463-8

Earth, Planets and Space

FULL PAPER Open Access

Estimation of ballistic block landing energy during 2014 Mount Ontake eruption

Kae Tsunematsu[1*], Yasuhiro Ishimine[2], Takayuki Kaneko[3], Mitsuhiro Yoshimoto[1], Toshitsugu Fujii[1] and Koshun Yamaoka[4]

Abstract

The 2014 Mount Ontake eruption started just before noon on September 27, 2014. It killed 58 people, and five are still missing (as of January 1, 2016). The casualties were mainly caused by the impact of ballistic blocks around the summit area. It is necessary to know the magnitude of the block velocity and energy to construct a hazard map of ballistic projectiles and design effective shelters and mountain huts. The ejection velocities of the ballistic projectiles were estimated by comparing the observed distribution of the ballistic impact craters on the ground with simulated distributions of landing positions under various sets of conditions. A three-dimensional numerical multiparticle ballistic model adapted to account for topographic effect was used to estimate the ejection angles. From these simulations, we have obtained an ejection angle of $\gamma = 20°$ from vertical to horizontal and $\alpha = 20°$ from north to east. With these ejection angle conditions, the ejection speed was estimated to be between 145 and 185 m/s for a previously obtained range of drag coefficients of 0.62–1.01. The order of magnitude of the mean landing energy obtained using our numerical simulation was 10^4 J.

Keywords: Ballistics, Mount Ontake, 3D multiparticle numerical model, Drag, Topographic effect

Introduction

Ballistic projectiles are ejected during explosive eruptions, follow a parabolic trajectory in the air that is minimally affected by wind, and ultimately land on the ground (Wilson 1972). These blocks can cause significant damage, such as penetrating roofs (Blong 1981, 1984; Ui et al. 2002), demolishing mountain huts, injuring humans (Blong 1984; Baxter and Gresham 1997), and causing fires if they are still hot when they land (Pistolesi et al. 2011). Our work on deducing the ejection conditions of ballistic projectiles and estimating their landing velocity and energy is useful for reducing the risk of damage caused by ballistic blocks ejected during volcanic eruptions.

The phreatic eruption of Mount Ontake, located in central Japan, began at 11:52 a.m. on September 27, 2014. The eruption left 58 people dead, and five people are still missing (as of January 1, 2016). The high number of casualties was the result of the numerous hikers around the summit area. According to the October 18, 2014, issue of the newspaper Shinano Mainichi Shimbun, there were at least 340 people around the summit area at the start of the eruption. The weather was fine, and people had arrived to enjoy the beautiful view of the colored autumn leaves on the mountain (Shinano Mainichi Shimbun Newspaper, October 18, 2014). Figure 1 shows a map of Mount Ontake and the surrounding area, and the numbers on the map indicate the number of casualties at each site. Nagano Police Office announced that 55 people died from lesions (damage from impacts), another died from thermal trauma, and the others' cause of death was unknown (Asahi Shimbun Digital on October 27, 2014). This implies that most of the casualties were caused by impacts from high-speed ballistic blocks. However, not all of the locations indicated on the map in Fig. 1 are the precise locations where the victims were struck by blocks. Some survivors explained that several of the victims were able to move themselves to other locations after they were injured (Shinano Mainichi Shimbun Newspaper, March 26, 2015).

*Correspondence: kae.tsunematsu@mfri.pref.yamanashi.jp
[1] Mount Fuji Research Institute, Yamanashi Prefectural Government, Japan, 5597-1 Kenmarubi Kamiyoshida, Fujiyoshida-shi, Yamanashi 403-0005, Japan
Full list of author information is available at the end of the article

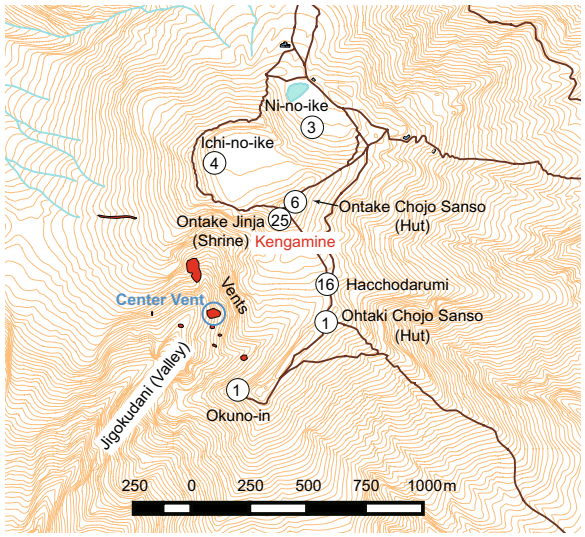

Fig. 1 Map of Mount Ontake with approximate positions of casualties based on journal reports (Asahi Shimbun Newspaper, October 27, 2014, p. 35; Yamanashi Nichinichi Shimbun Newspaper, September 26, 2015, p. 19). The *numbers on the map* represent the number of casualties at each site. The eruption left 58 people dead, and five people are still missing. The locations of the vents were taken from the Web site for the Geospatial Information Authority of Japan (2014). The position of the vent labeled "Center Vent" was used as the ejection position of ballistic blocks in our 3D multiparticle numerical simulations

To avoid such a high number of ballistic block-related casualties, it is useful to make hazard maps (Crandell et al. 1984; Alatorre-Ibargüengoitia et al. 2012; MIAVITA Team 2012; Fitzgerald et al. 2014), construct shelters around the crater of the volcano, and reinforce the roofs of mountain huts (Pomonis et al. 1999). To make a hazard map for volcanic ballistic projectiles, it is necessary to estimate the travel distance, landing velocity, and landing energy of the ballistic projectiles. Therefore, the objective of our project is to estimate the impact velocity and energy of ballistic projectiles when they land on the ground or impact the mountain huts. These estimations would also be useful in the design of shelters and the reinforcement of mountain hut roofs.

It is difficult to directly measure the impact speed and energy from monitoring data. Furthermore, no video equipment was set up in the summit area at the time of eruption. Although some hikers shot videos with their cameras or mobile phones, the location and time stamps of these videos were not clear or required calibration (Oikawa et al. 2016). For this reason, we implemented numerical simulations and compared the results with the distribution of impact craters to judge which initial conditions are most plausible for reproducing the existing distribution of impact craters. Some input parameter values were defined based on field observations or measurements of rocks sampled during the field observation.

Impact craters are often produced when ballistic blocks hit the ground. Several studies on impact craters have been conducted regarding the distribution of the ballistic blocks after landing (Fitzgerald et al. 2014; Pistolesi et al. 2008; Maeno et al. 2013). For the 2014 Mount Ontake eruption, Kaneko et al. (2016) studied the distribution of impact craters of ballistics from photographs they took days after the start of the eruption from a journalist's helicopter. They defined A, B, C, and D zones around the vent depending on the number of impact craters per 5 m × 5 m. These impact craters were visible because they formed on the fine ash layer during the eruption. Ballistic blocks were ejected several times on 27 September from 11:52 a.m. when the eruption started to 12:40 p.m. when the fall of pyroclasts ended (Oikawa et al. 2016). For this reason, the distributions obtained by Kaneko et al. (2016) likely exclude some blocks ejected before the ash deposition. To estimate the ejection speed of the ballistics, we compared the ground distribution of ballistic blocks simulated using our numerical model with the distribution of the impact craters photographed by Kaneko et al. (2016).

The characteristics of ballistic impact crater distribution featured in Kaneko et al. (2016) were first, it is elongated to the north-northeast direction, and second, the farthest impact crater is approximately 1 km from the vent around Ninoike pond. This is consistent with our field observation that the ballistic blocks that landed farthest from the vent were the blocks that fell on the Ninoike Honkan hut, which is located north of Ninoike pond.

The elongation of the distribution of impact craters may have been caused by a combination of an inclined ejection and topographic control. Topographic control is taken into consideration because the stretched direction of the Jigokudani valley is similar to the direction of the elongation of impact crater distribution and the eruptive vents are in the Jigokudani valley. Thus, the wall of the valley might have prevented the ballistic projectiles from flying out from the valley in some directions. An inclination is also considered in our study because no impact crater was found in the lower and southwest part of the vent (Kaneko et al. 2016). Ballistic blocks hardly drop on the south-southwestern slope if the ejection angle has an inclination. Although wind is another possible cause of this elongation, the wind at the height of the summit was weak (approximately 2–3 m/s) according to the weather monitoring data of the Japan Meteorological Agency. Therefore, it is unlikely that wind materially affected the transport of ballistic projectiles.

To clarify the reason for the elongated distribution of impact craters and deduce the ejection angles, we used our multiparticle three-dimensional numerical model which is able to calculate the trajectories and landing positions of ballistic projectiles based on the local topography. The ejection speed was then estimated based on these ejection angles, and once these ejection conditions were obtained, the ballistic landing velocity and energy was calculated.

Numerical models of ballistic projectiles have been developed since the 1940s. Minakami (1942) used an analytical ballistic equation to estimate the ejection speed of the 1937 Asama eruption. Wilson (1972) formulated a discretized numerical model for the trajectories of pyroclasts for the first time. Using a phreatomagmatic eruption as an example, Self et al. (1980) estimated an ejection velocity of 100–150 m/s for the 1977 Ukinrek Maars eruption. After these early studies, single-particle models mostly considered the drag effect of a vulcanian explosion (Fagents and Wilson 1993) or that of an eruption with a volcanic jet (Bower and Woods 1996). In the 2000s, some studies were dedicated to multiparticle numerical models (Saunderson 2008; de'Michieli Vitturi et al. 2010). Recently, Tsunematsu et al. (2014) proposed a numerical model with interparticle collisions but without drag. This model was the first to describe the two-dimensional (2D) deposited particle distribution on the ground, making the output data much more suitable for application to hazard maps. This study aims to calculate the particle trajectory and three-dimensional (3D) distribution on the ground, considering drag and topographic effects. Therefore, this model is adapted to evaluate the topographic effect which is not accounted for other numerical models. Using this improved numerical model, we estimated the ejection conditions and the landing velocity and energy of ballistic projectiles released during 2014 Mount Ontake eruption.

Methods

Our multiparticle numerical ballistics model consists of two calculations to determine the velocity and transport of the ballistic particles. The velocity equation is written with vectors for all directions as (Alatorre-Ibargüengoitia and Delgado-Granados 2006)

$$m\frac{\mathrm{D}\vec{\boldsymbol{v}}}{\mathrm{D}t} = -\frac{AC_{\mathrm{D}}\rho_{\mathrm{a}}(\vec{\boldsymbol{v}}-\vec{\boldsymbol{u}})|\vec{\boldsymbol{v}}-\vec{\boldsymbol{u}}|}{2} - m\vec{\boldsymbol{g}}, \quad (1)$$

where m is the mass of a ballistic block, A is the cross-sectional area of the block perpendicular to the flow direction, C_{D} is the drag coefficient, ρ_{a} is the air density, g is the acceleration due to gravity, v is the velocity of the block, and u is the velocity of the ambient gas flow. The velocity equation is solved for each particle, location, direction, and time step. Then, the transport of ballistic particles is calculated using the Lagrangian method as

$$\vec{\boldsymbol{r}} = \vec{\boldsymbol{r}}_0 + \vec{\boldsymbol{v}} \cdot \Delta t,$$

where $\boldsymbol{r}$ is the location of each block and Δt is the time step, which is constant throughout the simulation. All particles are assumed to be spherical. The particle velocity was calculated using the explicit Runge–Kutta method.

In the proposed multiparticle model, parameter values are set based on certain distributions, including the uniform, Gaussian, and power-law distributions. However, to reveal the effect of the parameter value, most parameters were set as constants in the simulation. The input parameters related to the properties of the particles are the particle diameter, particle density, and drag coefficient. Among these particle properties, only the particle density is set using the Gaussian distribution; the particle diameter and drag coefficient are given constant values. Other input parameters describe the ejection conditions; these include the ejection speed and the polar angle θ and azimuthal angle ϕ of the ejection velocity v_{e} (Fig. 2a). When a group of particles are ejected with a certain inclination, the ejection axis for the group can be defined by a rotation angle γ from the vertical axis (Fig. 2b). The group is also given a certain planar direction using the direction angle α, which is defined with respect to north and increases as the direction rotates toward the east, i.e., clockwise (Fig. 2c). Only a single instantaneous burst is considered in the simulation because it is impossible to recognize which impact crater was made by the first or second ejection pulse. Another parameter called the "gas flow effect range" L_{f} was used in the simulation to reproduce the gas ejected from the vent (Fig. 2d). This parameter is introduced to more realistically represent an explosion, in that the flow of the ejected gas, if within a certain range from the vent, likely affects particles. All parameters input into the simulation are given in Table 1. The method for obtaining the value of each parameter is explained in the remainder of this section.

Drag coefficient

The drag coefficient C_{D}, which is included in Eq. (1), is one of the most important parameters. The drag coefficient for a volcanic particle is strongly dependent on its shape (Wilson and Huang 1979) and Reynolds number (Mastin 2001; Alatorre-Ibargüengoitia and Delgado-Granados 2006; de'Michieli Vitturi et al. 2010). It is also dependent on its Mach number M_{a} if the flow is compressible and if $M_{\mathrm{a}} > 0.7$ (Mastin 2001; Alatorre-Ibargüengoitia and Delgado-Granados 2006). Alatorre-Ibargüengoitia and Delgado-Granados (2006) measured the drag coefficient for ballistic blocks by conducting

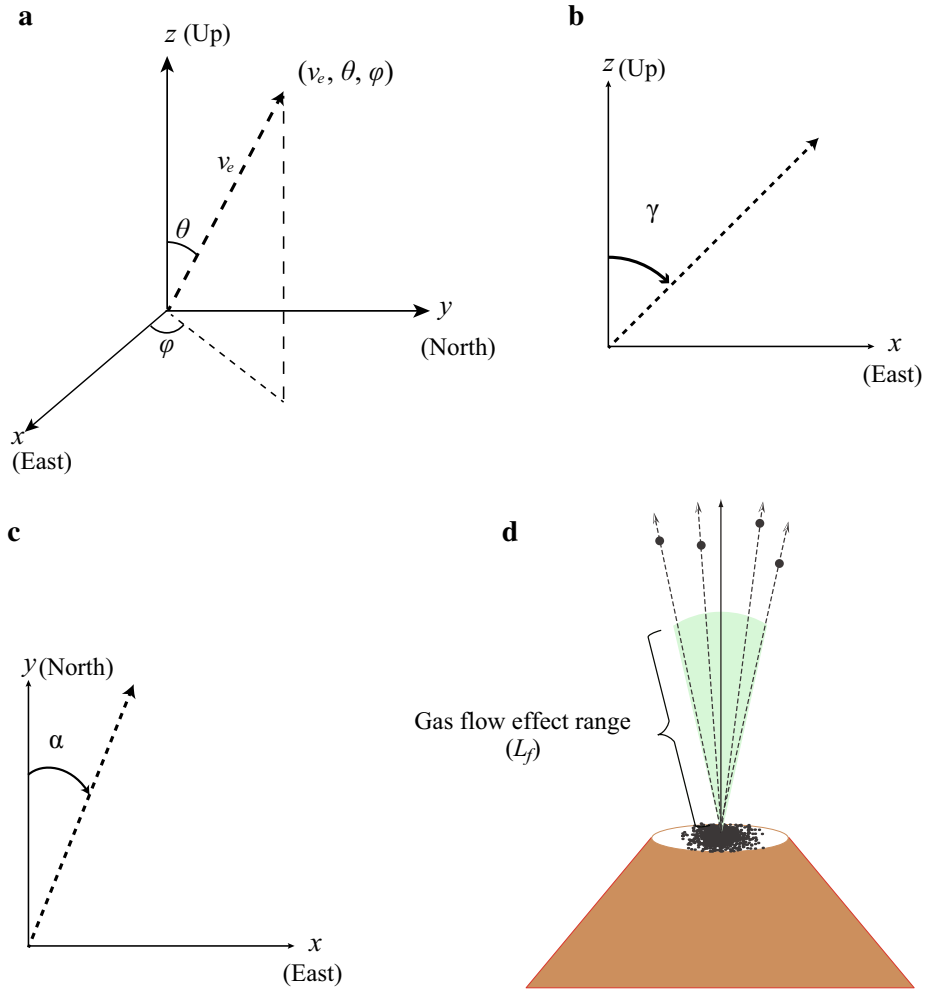

Fig. 2 Parameters related to ejection conditions. **a** Particle ejection speed v_e, polar angle θ, and azimuth angle φ. **b** Rotation angle γ. **c** Direction angle α from north. **d** Gas flow effect range L_f where gas flow is affecting the particle transport

wind tunnel experiments. They set the flow velocity to approximately 20 m/s, and the particles were blown by this flow in the wind tunnel. From these experiments, they obtained an average drag coefficient of 0.8, with the results of individual experiments ranging from 0.62 to 1.01. This measurement was conducted in a horizontal wind tunnel, and it was possible to mediate the effects of gravity, which usually create some noise in the measurement. Furthermore, the Reynolds number was kept within the turbulent range at all times, and drag separation was assumed not to occur during the experiment. Therefore, this range can be assumed to accurately represent the range of possible drag coefficients for the ballistic blocks. Recently, many other models have been proposed for calculating the drag coefficient considering different particle shapes (Dellino et al. 2005; Bagheri et al. 2013). Because these models focus only on volcanic ash particles and do not consider the effects of the Mach number, they are not applicable to the calculation of our ballistic blocks.

Therefore, to determine the best fit for the ejection conditions, such as the rotation angle (γ), direction angle (α), and ejection speed, the average drag coefficient $C_D = 0.8$ obtained by Alatorre-Ibargüengoitia and Delgado-Granados (2006) was mainly used. Possible ranges for the ejection speed, landing velocity, and landing energy were then discussed by varying the drag coefficient within the range of 0.62–1.01 obtained in the individual experiments by Alatorre-Ibargüengoitia and Delgado-Granados (2006).

The gas flow may affect the particle transport when the explosion occurs, especially around the vent. To assess this effect, the gas flow velocity around the vent was included in the simulation. The range in which the gas

Table 1 Input parameters, variable names, and values

Parameter name	Notation	Value
Particle diameter (m)	D_p	0.2
Drag coefficient	C_D	0.0–1.2
Particle density (kg/m^3)	ρ_p	Mean = 2300 Std = 300
Particle ejection speed (m/s)	v_e	100–200
Polar angle (°)	θ	Mean = 0 Std = 15
Azimuth angle (°)	φ	Uniform distribution 0–360
Rotation angle from the vertical axis (°)	γ	20–80
Direction angle from north to east (°)	α	10–30
Gas flow effect range (m)	L_f	100

In this model, the particle density and polar angle values are randomly selected from a Gaussian distribution with the given means and standard deviations (std), and the azimuth angle is randomly selected from a uniform distribution with a range of 0°–360°

flow may affect the particle transport (Fig. 2d) is the distance from the ejection position in which the flow velocity is included in the particle velocity calculation. This is a type of drag effect, as the flow velocity is implemented in the drag term of Eq. (1).

The gas flow effect range was set to 100 m for all simulations because the pyroclastic cone that formed around the center vent was approximately 200 m in diameter (vent "J4" of Fig. 2 in Kaneko et al. 2016). This suggests that the explosive gas flow affected the particles within this area. However, the gas flow effect range is outside the scope of this study because the objective of this study is to ascertain which parameters significantly affect the ejection and landing conditions. In fact, the gas flow effect range changes less than 10 % of maximum travel distance when it is doubled in our trial simulation.

Particle density

For the initial conditions of our model, the particle density was measured in a laboratory. Five blocks were sampled by the joint observation group of the 2014 Mount Ontake eruption. Six rock samples, which were obtained by the members of the Joint Survey Team of the Japanese Coordinating Committee for Prediction of Volcanic Eruptions, were weighed in ambient air and in water. Then, the density was calculated based on the method by Shea et al. (2010) but without wrapping film because our samples were not overly vesiculated. Furthermore, the blocks were not cut into pieces, as the purpose of obtaining the particle density was to apply the values of the complete block to the numerical simulation.

The densities of the five samples ranged from 2020 to 2700 kg/m^3, and the average density was 2283 kg/m^3. Therefore, the mean density and its standard deviation were set to 2300 and 300 kg/m^3, respectively, in our simulator.

Particle diameter

The lengths along the three axes of the rocks sampled around the summit area were measured, and the arithmetic and geometric means (Biass and Bonadonna 2011) of these three dimensions were calculated for each rock. The average of the arithmetic means was 17.4 cm with a standard deviation of 8.1 cm, and the average of the geometric means was 16.8 cm with a standard deviation of 8.1 cm.

During our field observation, the diameter of the largest block we found was 70 cm, and particles of 10 cm in diameter were found on the wall of the mountain hut. Blocks that penetrated the roofs of mountain huts were approximately 20 cm in diameter.

Based on our direct measurement of the sampled blocks and the field observation, the most damaging particles in the 2014 Mount Ontake eruption were those of 20 cm in diameter. Thus, we used only 20-cm particles to investigate the ejection conditions and estimate the landing velocity and energy.

Vent position and ejection points

Several vents opened on September 27, 2014, according to reports by the Geospatial Information Authority of Japan (GSI) and Kaneko et al. (2016). Based on photographs of the summit area (Asahi Shimbun Newspaper, September 28, 2014; Kaneko et al. 2016), only one vent located in the center of these vents emitted an ash-laden plume, whereas the others emitted only steam-dominated plumes. The location of this center vent is shown in Fig. 1. We infer that the center vent was the only vent associated with the ejection of solid material by an ash-laden plume. Moreover, there is a pyroclastic cone in the south slope of the vent labeled "J4" by Kaneko et al. (2016), which corresponds to our center vent. This pyroclastic cone suggests that the center vent emitted ballistic blocks. Therefore, the center vent was set as the only vent that ejected ballistic blocks in our simulation. The location of the center vent was taken from the polygon file provided on the GSI Web site (Geospatial information authority of Japan 2014), and its center was used as the ejection position of the ballistic blocks. Although our ballistic simulator can accept multiple ejection positions, only one position was used to focus on the effects of the topography and the ejection direction on the distribution of deposited particles. The center vent and two other vents were in the Jigokudani valley (Kaneko et al. 2016). The Jigokudani valley runs from northeast to southwest. The shape of this valley and the ejection position

may have strongly affected the transport of the ballistic blocks.

Digital elevation model

To include the effect of topography, we used the digital elevation model (DEM), which was downloaded from the Web site for the National Land Numerical Information Download Service (National Land Information Division, MILT, Japan, 1974–2014). The DEM segments the land in a grid of 10 m in longitude and 10 m in latitude. Its coordinate system was the World Geodetic System 1984 (WGS84), and the coordinates were expressed as sets of latitude and longitude. The DEM based on WGS84 was converted into the Universal Transverse Mercator (UTM) coordinate system with the Geospatial Data Abstraction Library (GDAL) software using the bilinear method. This method is the recommended method for converting from WGS to UTM coordinates because of its small artifact in this type of conversion (Price 2013).

Results and discussion

Our multiparticle simulation calculated the trajectories of each particle using the DEM with given ejection conditions (Table 1; Figs. 3, 4, 5, 6, 7, 8). To investigate the ejection conditions, simulations were first conducted with various direction and rotation angles. Simulations were then performed with the direction and rotation angles that best matched the observed particle dispersion to assess the effect of the drag coefficient and ejection speed on the deposition of ballistic blocks.

Direction angle

According to Fig. 6 of Kaneko et al. (2016), the distribution of impact craters was elongated in the north-northeast direction. This elongation direction roughly measured on the map was approximately 17° from north. Presumably, the reasons for this elongation are the inclination of the ejection axis and the topographic control around the vent. Therefore, simulations with various direction angles α (Fig. 2c) were first conducted. Figure 4 shows the simulated distributions of deposit particles for direction angles of $\alpha = 10°$, 20°, and 30°. The resulting particle distributions were confined along the eastern edge, especially in the case of a direction angle of $\alpha = 30°$. The level of confinement decreased as the ejection direction shifted northward. Conversely, the distribution of deposited particles on the western side was dispersed.

During our field observation, we found several ballistic blocks that had penetrated the roof of the mountain hut Otaki Chojo Sanso (Cabinet Office, Japan 2015), and some hikers were hit by a shower at Otaki Chojo (Shinano Mainichi Shimbun 2015). Furthermore, many large blocks were dispersed along the Hacchodarumi trail

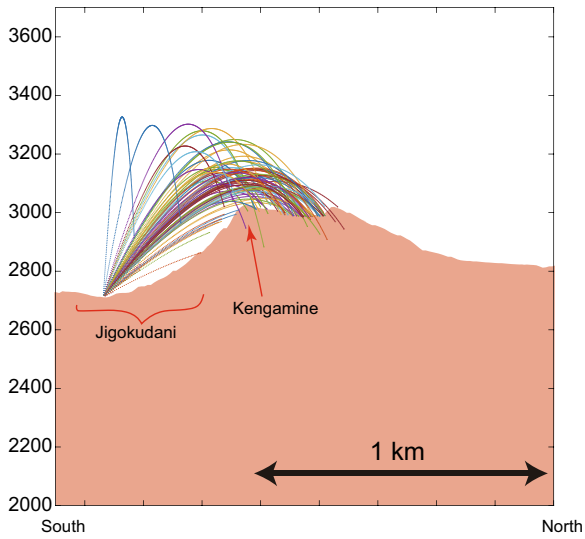

Fig. 3 Projection of all particle trajectories onto the north–south cross section, including center vent position. The simulation with our 3D multiparticle numerical model used the digital elevation model (DEM). The ejection speed of the particles was 150 m/s, and the rotation and direction angles were both 20°. A drag coefficient of $C_D = 0.8$ was used to simulate the trajectories. The trajectories are shown in *different colors* simply to allow the visualization of different particles; that is, the *colors* do not correspond to any specific value

(Oikawa et al. 2016). However, in the simulation with a direction angle of $\alpha = 30°$, no particle reached the Otaki Chojo Sanso hut or the Hacchodarumi trail (Fig. 4c). Conversely, many particles reached the Otaki Chojo Sanso hut and the Hacchodarumi trail when the direction angle was set to $\alpha = 20°$ (Fig. 4b). When the direction angle was set to $\alpha = 10°$ (Fig. 4a), fewer particles were deposited in the area around the Hacchodarumi trail, and more particles were deposited in the northwest of Ichinoike depression, where few impact craters were found in aerial observations (Kaneko et al. 2016). Given these results, the simulation with a direction angle of $\alpha = 20°$ best reproduced the actual distribution of deposited ballistic blocks.

Rotation angle

The rotation angle γ (Fig. 2b) was then varied to assess the effect of the inclination of the ejection axis. Simulations were conducted with the rotation angle varying from $\gamma = 20°$ to 80° (Fig. 5). The dispersion of the deposition decreased with increasing rotation angle, i.e., with increasing ejection axis inclination. The particle distribution in the Ichinoike depression was concentrated in the northeastern part when the rotation angle was between $\gamma = 40°$ and 80° (Fig. 5b–d). The cause of this inhomogeneity may be the uphill slope on the western side of the Ichinoike depression. When the particles were ejected

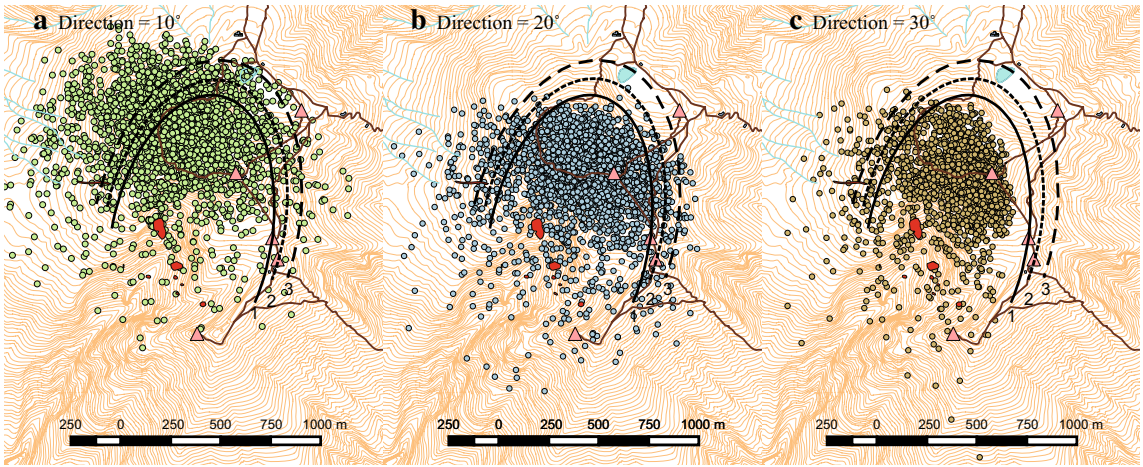

Fig. 4 Simulated distributions of deposited particles with direction angles of **a** $\alpha = 10°$, **b** $\alpha = 20°$, and **c** $\alpha = 30°$. Numerical simulations were performed with an ejection speed of $v_e = 150$ m/s, a rotation angle of $\gamma = 20°$ from the *vertical axis*, and a drag coefficient of $C_D = 0.8$. Each simulation used 3000 particles. *Black lines* in the map are the boundaries of the zones based on the concentration of impact craters, as reported by Kaneko et al. (2016) in order to compare simulated particle distribution with actual distribution of ballistic impact craters. Zone A is the area inside *line 1*. Zone B is the area between *lines 1* and *2*. Zone C is the area between *lines 2* and *3*. Zone D is the area outside the *line 3*

northeastward, some particles could not go beyond the southwestern ridge of the Ichinoike depression and were thus deposited on its southwestern slope. Other particles which were able to go beyond that slope were deposited in the northern region of the Ichinoike depression. Thus, only a small number of particles ejected with a rotation angle of $\gamma = 80°$ were deposited in the Ichinoike depression (Fig. 5d).

Based on the photographs taken by Kaneko et al. (2016), impact craters were homogeneously dispersed in the Ichinoike depression. Among the results shown in Fig. 5, only those of the simulation with a rotation angle of $\gamma = 20°$ show a homogenous dispersion of the deposited particles in the Ichinoike depression. As stated in the previous section, many ballistic blocks fell along the Hacchodarumi trail and around the Otaki Chojo Sanso hut during the actual eruption. In the simulations with rotation angles of $\gamma = 40°$, 60°, and 80°, few particles were deposited around the Hacchodarumi trail and the Otaki Chojo Sanso hut. Thus, the rotation angle that yields the distribution most closely resembling the observation is $\gamma = 20°$ from the vertical axis.

Ejection speed

Because the air drag on the particles was difficult to estimate, as described in Introduction, we performed simulations with various drag coefficients.

In Fig. 6, the 99th percentile of the travel distance is plotted for particle ejection speeds ranging from 100 to 200 m/s and drag coefficients ranging from 0.0 to 1.2. In theory, to consider the maximum travel distance, the 100th percentile of the travel distance should be calculated from the simulated deposition locations. However, in some cases, an outlier particle travels much farther than other particles. To reduce the influence of outlier particles, the 99th percentile was used to show the longest travel distance. To calculate the 99th percentile of the travel distance, the travel distances of the ejected particles were measured from their distances from the vent. When the number of counted particles reached 99 % of the total number of particles, this particle's travel distance was defined as the 99th percentile of the travel distance.

In Fig. 6, the different lines show the results of simulations with different drag coefficients C_D, and the black dashed line shows the largest observed distance between an impact crater and the center vent, which is approximately 1000 m (Kaneko et al. 2016). Thus, the ejection speed that is read from the intersections between the black dashed line and the solid colored lines gives the estimated ejection speed for each considered drag coefficient.

Assuming the drag coefficient was in the range of the experimental results obtained by Alatorre-Ibargüengoitia and Delgado-Granados (2006), which is 0.62–1.01, the estimated ejection speed was between approximately 145 and 185 m/s. This estimation is based on the assumption that no particle was transported by the plume. However, there were many photographs showing plumes between 11:52 a.m. and 12:40 p.m. when pyroclasts were falling (Oikawa et al. 2016), and the ballistic blocks may have been blown upward by the plume. The travel distance

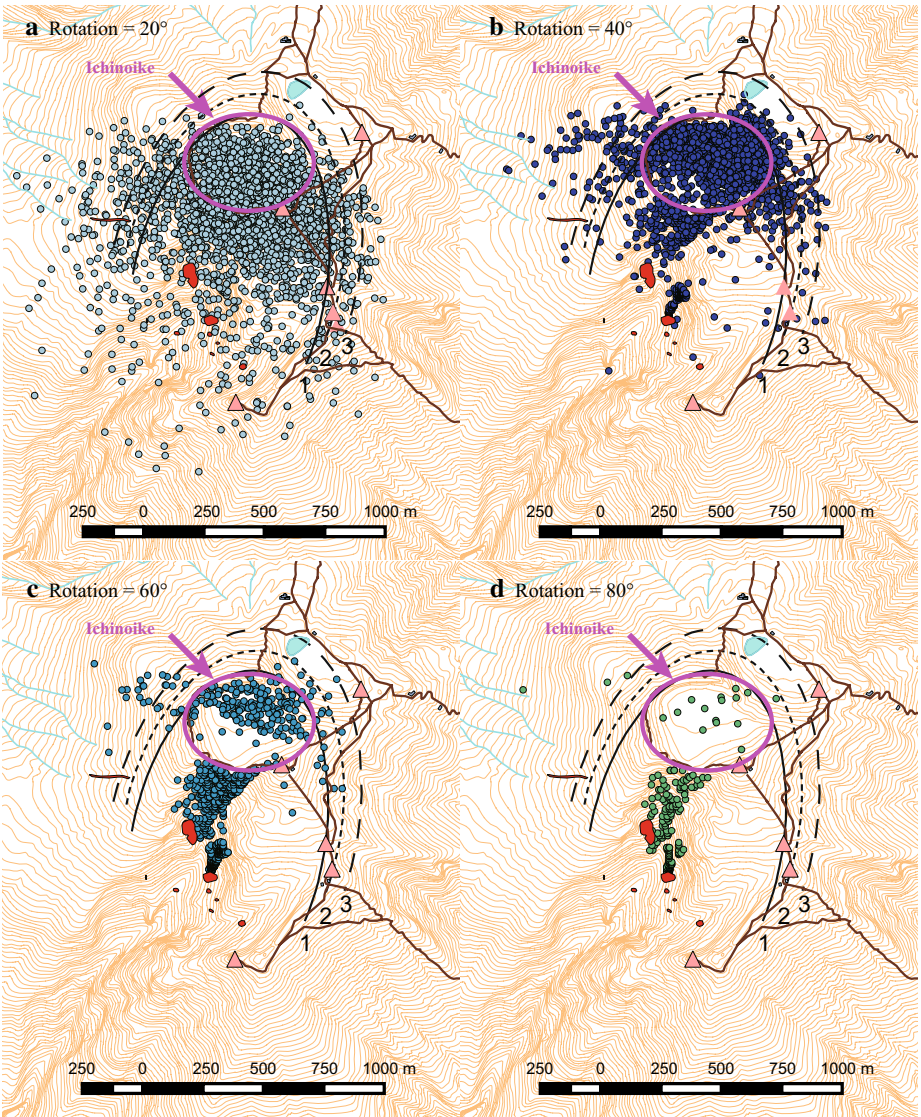

Fig. 5 Simulated distributions of deposited particles with rotation angles of **a** $\gamma = 20°$, **b** $\gamma = 40°$, **c** $\gamma = 60°$, and **d** $\gamma = 80°$. Numerical simulations were performed with an ejection speed of $v_e = 150$ m/s, a direction angle of $\alpha = 20°$ from the north, and a drag coefficient of $C_D = 0.8$. Each simulation used 3000 particles. *Black lines* are the boundaries of the impact crater zones, as reported by Kaneko et al. (2016) (see the caption of Fig. 4)

may have increased if the ballistic blocks were affected by the uprising plume. Therefore, the model could be overestimating the ejection velocity.

In contrast, Kaneko et al. (2016) estimated an ejection speed of 108 m/s using the program Eject! because they used a drag coefficient of approximately 0.1 based on the temperature at sea level (25 °C) and the thermal lapse rate (6.5 °C/km). To illustrate that our model is consistent with Eject!, the ejection speed was estimated to be approximately 110 m/s in the case of $C_D = 0.1$ as shown in Fig. 6. Given that the variation in the estimated ejection speed with a varying drag coefficient is large, defining the drag coefficient is very important for discussing the travel distances of ballistic projectiles. In addition, the effects of the plume or gas velocity should be seriously considered in numerical simulations in future studies.

Landing velocity and energy

Figures 7 and 8 show the mean landing velocity and energy, respectively. To estimate the landing velocities and energies, only drag coefficients in the range of 0.6–1.2 were used based on the range obtained by Alatorre-Ibargüengoitia and Delgado-Granados (2006). The mean landing velocity was calculated based on the simulation

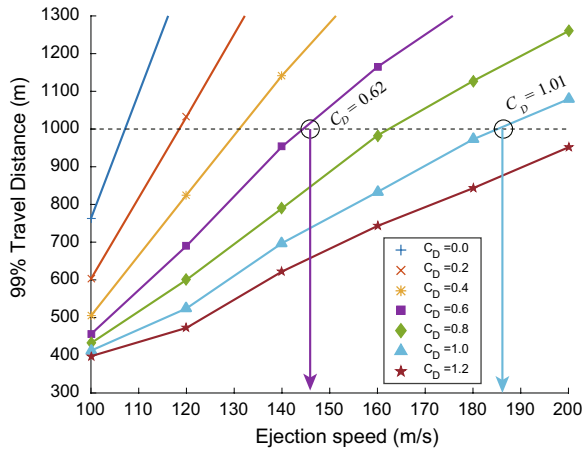

Fig. 6 Simulated 99th percentiles of the travel distance for drag coefficients C_D ranging from 0.0 to 1.2. *The dashed line* indicates the largest observed distance between an impact crater and the center vent (Kaneko et al. 2016). The rotation and direction angles were both 20°. Each simulation used 10,000 particles

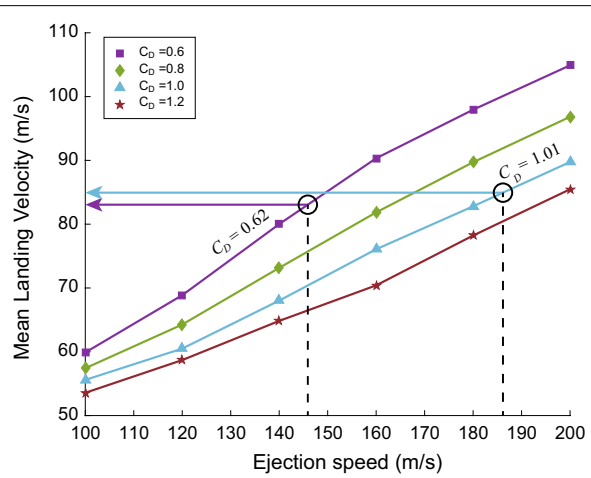

Fig. 7 Simulated mean landing velocity for drag coefficients C_D ranging from 0.6 to 1.2. The rotation and direction angles were both 20°. Each simulation used 10,000 particles

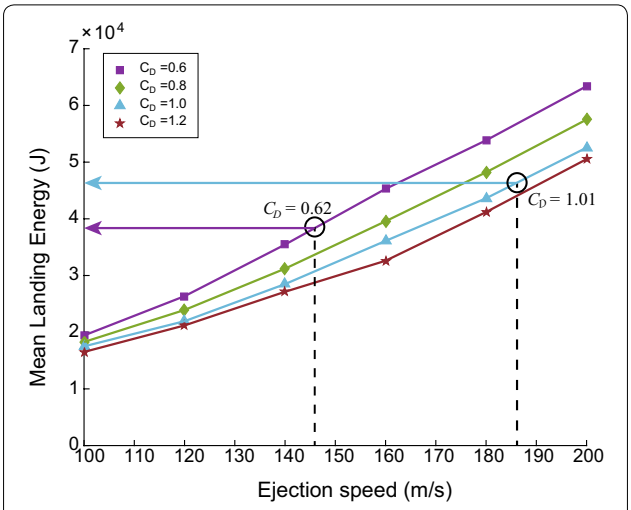

Fig. 8 Simulated mean landing energy for drag coefficients C_D ranging from 0.6 to 1.2. The rotation and direction angles were both 20°. Each simulation used 10,000 particles

results for 10,000 particles with the estimated rotation angle $\gamma = 20°$ and direction angle $\alpha = 20°$. The mean landing velocities with all considered drag coefficients were lower than the ejection speeds (Fig. 7). The particle velocity was significantly reduced by the drag effect in our simulations.

Based on our estimation of the ejection speed in the previous section, the ejection speeds were approximately $v_e = 145$ and 185 m/s with drag coefficients of $C_D = 0.62$ and 1.01, respectively. In Fig. 7, the results for $C_D = 0.6$ and 1.0 at ejection speeds of 145 and 185 m/s give mean landing velocities of 83 and 85 m/s, which correspond to 299 and 306 km/h, respectively. These landing velocities are smaller than the ejection velocities estimated with the given drag coefficients because the drag reduces particle velocity.

The mean landing energy was also calculated based on the simulation results with 10,000 particles. The landing energy was calculated as

$$E_l = \frac{1}{2} m v_l^2, \tag{2}$$

where E_l is the landing energy and v_l is the landing velocity. Based on Fig. 8, the landing energy was estimated to be 3.8×10^4 and 4.5×10^4 J for $v_e = 145$ m/s and $C_D = 0.6$ and for $v_e = 185$ m/s and $C_D = 1.0$, respectively. These energies are the same order of magnitude (10^4 J) as the critical value of ballistic blocks penetrating the reinforced concrete (RC) roof, as estimated by Spence et al. (2005). Spence et al. (2005) also presented a plot of the critical energy of ballistic blocks penetrating a plywood roof and demonstrated that the order of magnitude of this energy is in the range of 10^2–10^3 J. All huts around the summit area of Mount Ontake are made of wood, and the energies estimated by our simulations are much larger than the critical energy required to penetrate a wooden roof. Therefore, in theory, most blocks would have penetrated the roofs of the mountain huts. However, some 20-cm blocks did not fully penetrate the roofs they struck and were still lodged in the roofs when we investigated the huts around the summit area. The mean value of particle mass is 9.6 kg calculated based on the mean value of density of 2300 kg/m^3 and the particle diameter of 0.2 m assuming that the particles are spherical. If the

particle diameter is 0.1 m, the particle mass would be 1.2 kg. Thus, the landing energy could be roughly one order smaller if the particle size is half because the landing energy is proportional to the particle mass as shown in Eq. (2). It is possible that some particles are not penetrated the roofs because the particle size was small and the impact energy was also so small that the particle did not penetrated the roof.

Spence et al. (2005) did not discuss whether the energy is dependent on the particle size; however, it should be noted that the energy likely varies with the particle size, as the drag term in Eq. (1) depends on the particle mass and the cross-sectional area of the block. So far, criteria for roof penetration can be found only in studies by Blong (1984), Pomonis et al. (1999), and Spence et al. (2005), and similar values were found in all three studies. To discuss the possibility of roof penetration, more realistic critical values must be derived from observations or laboratory experiments (Williams 2016).

Furthermore, our estimation did not consider variation in the block size, and we ignored the possibility of particles being blown upward by volcanic plumes or the blasts, which may have affected the transport of blocks. One future objective may be to find the block size distribution on the ground and combine our ballistic model with a plume or blast model to obtain a more realistic estimation of the landing energy.

Conclusions

Using a 3D numerical multiparticle model of ballistic blocks, the ejection conditions of the 2014 Mount Ontake eruption, such as particle speed and rotation and direction angles, were estimated by comparing the simulated landing position distributions obtained using various sets of conditions with the distribution of ballistic impact craters obtained by Kaneko et al. (2016). The mean landing velocity and energy were then calculated for a range of possible drag coefficients using the estimated ejection conditions.

The topographic control is considered with our modified numerical model, and a rotation angle of $\gamma = 20°$ from the vertical axis and a direction angle of $\alpha = 20°$ from the north were successfully derived by comparing our simulated particle distribution with the shape and axis of distribution of the impact craters observed by Kaneko et al. (2016).

The ejection speed was determined to be between 145 and 185 m/s for drag coefficients ranging from 0.62 to 1.01; this range was proposed by Alatorre-Ibargüengoitia and Delgado-Granados (2006) based on their laboratory experiments. The mean landing velocity is always lower than the ejection speed, and the estimated mean landing velocity of 10,000 particles with ejection speeds ranging from 145 to 185 m/s was found to be between 83 and 85 m/s. The simulated mean landing energies were larger than the critical energy of roof penetration for a plywood roof, and the value ranged from 3.8×10^4 to 4.5×10^4 J.

These values, estimated by comparing the simulated distribution of deposited particles with the observed distribution of impact craters, do not consider all the ballistic projectiles released from the vent of the 2014 Mount Ontake eruption because the impact craters were formed after fine tephra was deposited on the ground, which may have occurred after the initial ejection of ballistic blocks.

Authors' contributions

KT simulated ballistic trajectories and wrote the manuscript. YI checked the numerical code and simulated results. TK offered the photographs and the data of impact craters, and MY offered the ballistic block sample from the field. TF and KY discussed and helped to write the manuscript. KT, YI, and MY joined the ground truth of the summit area. All authors read and approved the final manuscript.

Author details

[1] Mount Fuji Research Institute, Yamanashi Prefectural Government, Japan, 5597-1 Kenmarubi Kamiyoshida, Fujiyoshida-shi, Yamanashi 403-0005, Japan. [2] National Institute of Public Health, Japan, 2-3-6 Minami, Wako-shi, Saitama 351-0197, Japan. [3] Earthquake Research Institute, The University of Tokyo, 1-1-1 Yayoi, Bunkyo-ku, Tokyo 113-0032, Japan. [4] Graduate School of Environmental Studies, Nagoya University, Furo-cho, Chikusa-ku, Nagoya 464-8601, Japan.

Acknowledgements

This study was supported by the Ministry of Education, Culture, Sports, Science and Technology (MEXT) and the Japan Society for the Promotion of Science (JSPS) KAKENHI Grant Number 15K01256 and 23241055. Kae Tsunematsu and Yasuhiro Ishimine studied in the restricted summit area of Mount Ontake with the support and special permission of the Cabinet Office of Japan. Mitsuhiro Yoshimoto was a member of the Joint Survey Team of the Japanese Coordinating Committee for Prediction of Volcanic Eruptions. We appreciate Japan Meteorological Agency's support providing wind data around the summit of Mount Ontake. We thank the town of Kiso and the village of Otaki in Nagano Prefecture for permitting our field survey around the summit area. We thank Marcus Bursik for his useful advice. We are grateful for the detailed comments and thorough reviews from Ben Kennedy and another anonymous reviewer, and the great help from the editor, Nobuo Geshi.

Competing interests

The authors declare that they have no competing interests.

Received: 30 November 2015 Accepted: 6 May 2016
Published online: 25 May 2016

References

Alatorre-Ibargüengoitia MA, Delgado-Granados H (2006) Experimental determination of drag coefficient for volcanic materials: calibration and application of a model to Popocatépetl volcano (Mexico) ballistic projectiles. Geophys Res Lett 33(11):L11302

Alatorre-Ibargüengoitia MA, Delgado-Granados H, Dingwell DB (2012) Hazard map for volcanic ballistic impacts at Popocatépetl volcano (Mexico). Bull Volcanol 74:2155–2169. doi:10.1007/s00445-012-0657-2

Asahi Shimbun Digital (2014) 90 percent of victims died instantly. Were a half of them hit directly by the blocks? Dead body inspection. Asahi Shimbun Digital, 27 Oct 2014

Asahi Shimbun Newspaper (2014) The vent of Mount Ontake blowing up a volcanic plume. Asahi Shimbun, 28 Sept 2014

Asahi Shimbun Newspaper (2014) Mount Ontake eruption. At that time…. Asahi Shimbun, 27 Oct 2014

Bagheri GH, Bonadonna C, Manzella I (2013) Dedicated vertical wind tunnel for the study of sedimentation of non-spherical particles. Rev Sci Instrum 84:054501. doi:10.1063/1.4805019

Baxter PJ, Gresham A (1997) Deaths and injuries in the eruption of Galeras Volcano, Colombia, 14 January 1993. J Volcanol Geotherm Res 77:325–338

Biass S, Bonadonna C (2011) A quantitative uncertainty assessment of eruptive parameters derived from tephra deposits: the example of two large eruptions of Cotopaxi volcano, Ecuador. Bull Volcanol 73:73–90

Blong RJ (1981) Some effects of tephra falls on buildings. In: Self S, Sparks RSJ (eds) Tephra studies: proceedings of the NATO advanced study institute Tephra Studies as a Tool in Quaternary Research

Blong RJ (1984) Volcanic hazards: a sourcebook on the effects of eruptions. Academic Press, London

Bower S, Woods A (1996) On the dispersal of clasts from volcanic craters during small explosive eruptions. J Volcanol Geotherm Res 73:19–32

Cabinet Office, Japan (2016) Handbook for an enhancement of shelters on active volcanoes. Disaster Management section of Cabinet Office, Japan. Retrieved, 1 January, 2016, from http://www.bousai.go.jp/kazan/shiryo/ **(in Japanese)**

Crandell DR, Booth B, Kusumadinata K, Shimozuru D, Walker GPL, Westercamp D (1984) Source-book for volcanic-hazards zonation. UNESCO, Paris

de'Michieli Vitturi M, Neri A, Esposti Ongaro T, Lo Savio S, Boschi E (2010) Lagrangian modeling of large volcanic particles: application to vulcanian explosions. J Geophys Res 115(B8):B08206

Dellino P, Mele D, Bonasia R, Braia G, La Volpe L, Sulpizio R (2005) The analysis of the influence of pumice shape on its terminal velocity. Geophys Res Lett 32:2–5. doi:10.1029/2005GL023954

Fagents SA, Wilson L (1993) Explosive volcanic eruptions: VII. The ranges of pyroclasts ejected in transient volcanic explosions. Geophys J Int 113:359–370

Fitzgerald RH, Tsunematsu K, Kennedy BM, Breard ECP, Lube G, Wilson TM, Jolly AD, Pawson J, Rosenberg MD, Cronin SJ (2014) The application of a calibrated 3D ballistic trajectory model to ballistic hazard assessments at Upper Te Maari, Tongariro. J Volcanol Geotherm Res 286:248–262. doi:10.1016/j.jvolgeores.2014.04.006

Geospatial Information Authority of Japan (2016) Acts of GSI, Japan for the Mount Ontake 2014 eruption. Retrieved 12 February, 2016, from http://www.gsi.go.jp/BOUSAI/h26-ontake-index.html

Kaneko T, Maeno F, Nakad S (2016) 2014 Mount Ontake eruption: Characteristics of the phreatic eruption as inferred from aerial observations. Earth Planets Space 68:72. doi:10.1186/s40623-016-0452-y

Maeno F, Nakada S, Nagai M, Kozono T (2013) Ballistic ejecta and eruption condition of the vulcanian explosion of Shinmoedake volcano, Kyushu, Japan on 1 February, 2011. Earth Planets Space 65:609–621

Mastin LG (2001) A simple calculator of ballistic trajectories for blocks ejected during volcanic eruptions. U.S. Geological Survey Open-File Report 01-45, 16 pp. Retrieved 1 January, 2016 from http://pubs.usgs.gov/of/2001/0045/

MIAVITA (2012) Handbook for volcanic risk management: Prevention, crisis management, resilience. MIAVITA Team, Orleans

Minakami T (1942) On the distribution of volcanic ejecta (part I): the distributions of volcanic bombs ejected by the recent explosions of Asama. Bull Earthq Res Inst Univ Tokyo 20:65–91

National Land Information Division (1974–2014) National spatial planning and regional policy Bureau, MILT, Japan. National Land Numerical Information download service. Retrieved 1 January, 2016, from http://nlftp.mlit.go.jp/ksj-e/

Oikawa T, Yoshimoto M, Nakada S, Maeno F, Komori J, Shimano T, Takeshita Y, Ishizuka Y, Ishimine Y (2016) Reconstruction of the 2014 eruption sequence of Ontake Volcano (Ontake-san) from recorded images and interviews. Earth Planets Space. doi:10.1186/s40623-016-0458-5

Pistolesi M, Rosi M, Pioli L, Renzulli A, Bertagnini A, Andronico D (2008) The paroxysmal event and its deposits. In: Calvari S, Inguaggiato S, Puglisi G, Ripepe M, Rosi M (eds) The Stromboli volcano: an integrated study of the 2002–2003 eruption. American Geophysical Union, Washington, DC. doi:10.1029/182GM26

Pistolesi M, Delle Donne D, Pioli L, Rosi M, Ripepe M (2011) The 15 March 2007 explosive crisis at Stromboli volcano, Italy: assessing physical parameters through a multidisciplinary approach. J Geophys Res 116(B12206):2011. doi:10.1029/2011JB008527

Pomonis A, Spence RJS, Baxter PJ (1999) Risk assessment of residential buildings for an eruption of Furnas Volcano, São Miguel, the Azores. J Volcanol Geotherm Res 92:107–131

Price M (2013) Looking good—properly reprojecting elevation rasters. ArcUser Esri, fall 2013. Retrieved 1 January, 2016, from http://www.esri.com/esri-news/arcuser/fall-2013/looking-good

Saunderson HC (2008) Equations of motion and ballistic paths of volcanic ejecta. Comput Geosci 34:802–814. doi:10.1016/j.cageo.2007.10.004

Self S, Kienle J, Huot JP (1980) Ukinrek Maars Alaska, II. Deposits and formation of the 1977 craters. J Volcanol Geotherm Res 7:39–65

Shea T, Houghton BF, Gurioli L, Cashman KV, Hammer JE, Hobden BJ (2010) Textural studies of vesicles in volcanic rocks: an integrated methodology. J Volcanol Geotherm Res 190:3–4

Shinano Mainichi Shimbun (2015) Verification of Mount Ontake eruption—living with a volcano. What do we learn from 9.27?. The Shinano Mainichi Shimbun Press, Nagano **(in Japanese)**

Shinano Mainichi Shimbun Newspaper (2014) Hit of an Eruption (1)—difficulty in initial action of the rescue at high altitude. Shinano Mainichi Shimbun, 18 Oct 2014 **(in Japanese)**

Shinano Mainichi Shimbun Newspaper (2015) Estimation of damaged area of lost 6 people. One year after the eruption. Shinano Mainichi Shimbun, 26 Mar 2015 **(in Japanese)**

Spence RJS, Kelman I, Baxter PJ, Zuccaro G, Petrazzuoli S (2005) Residential building and occupant vulnerability to tephra fall. Nat Hazards Earth Syst Sci 5(4):477–494

Tsunematsu K, Chopard B, Falcone J, Bonadonna C (2014) A numerical model of ballistic transport with collisions in a volcanic setting. Comput Geosci 63:62–69

Ui T, Nakagawa M, Inaba C, Yoshimoto M (2002) Sequence of the 2000 eruption. Bulletin of the Volcanological Society of Japan, Usu Volcano **(in Japanese)**

Williams G (2016) The vulnerability of Auckland city's buildings to tephra hazards. Master thesis, University of Canterbury, Christchurch, New Zealand

Wilson L (1972) Explosive volcanic eruptions-II. The atmospheric trajectories of pyroclasts. Geophys J R Astr Soc 30:381–392

Wilson L, Huang TC (1979) The influence of shape on the atmospheric settling velocity of volcanic ash particles. Earth Planet Sci Lett 44:311–324

Yamanashi Nichinichi Shimbun Newspaper (2015) One year after Mount Ontake eruption. Yamanashi Nichinichi Shimbun, 26 Sept 2015 **(in Japanese)**